ACS APPLIED MATERIALS & INTERFACES

www.acsami.org

Research Article

NH_3 Sensor Based on 2D Wormlike Polypyrrole/Graphene Heterostructures for a Self-Powered Integrated System

Jianmei Gao,[⊥] Jieqiong Qin,[⊥] Junyu Chang, Hanqing Liu, Zhong-Shuai Wu,* and Liang Feng*

Cite This: *ACS Appl. Mater. Interfaces* 2020, 12, 38674−38681

Read Online

ACCESS | Metrics & More | Article Recommendations | Supporting Information

ABSTRACT: The rapid development of a NH_3 sensor puts forward a great challenge for active materials and integrated sensing systems. In this work, an ultrasensitive NH_3 sensor based on two-dimensional (2D) wormlike mesoporous polypyrrole/reduced graphene oxide (w-mPPy@rGO) heterostructures, synthesized by a universal soft template method is reported, revealing the structure−property coupling effect of the w-mPPy/rGO heterostructure for sensing performance improvement, and demonstrates great potential in the integration of a self-powered sensor system. Remarkably, the 2D w-mPPy@rGO heterostructrure exhibits preferable response toward NH_3 ($\Delta R/R_0$ = 45% for 10 ppm NH_3 with a detection limit of 41 ppb) than those of the spherical mesoporous hybrid (s-mPPy@rGO) and the nonporous hybrid (n-PPy@rGO) due to its large specific surface area (193 m^2/g), which guarantees fast gas diffusion and transport of carriers. Moreover, the w-mPPy@rGO heterostructures display outstanding selectivity to common volatile organic compounds (VOCs), H_2S, and CO, prominent antihumidity inteference superior to most existing chemosensors, superior reversibility and favorable repeatability, providing high potential for practicability. Thus, a self-powered sensor system composed of a nanogenerator, a lithium-ion battery, and a w-mPPy@rGO-based sensor was fabricated to realize wireless, portable, cost-effective, and light-weight NH_3 monitoring. Impressively, our self-powered sensor system exhibits high response toward 5−40 mg NH_4NO_3, which is a common explosive to generate NH_3 via alkaline hydrolysis, rendering it a highly prospective technique in a NH_3-based sensing field.

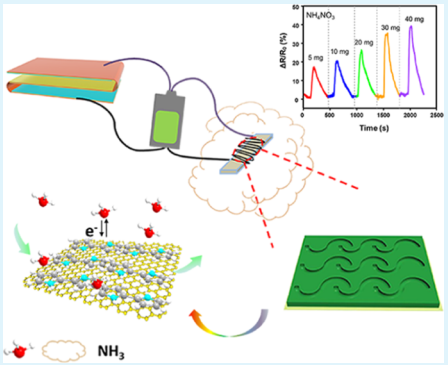

KEYWORDS: *ultrasensitive, wormlike mesoporous, polypyrrole/graphene heterostructures, high response, self-powered integrated system*

INTRODUCTION

With the rapid development of the industry, uncontrolled emission of hazardous gas makes environmental problems much more serious and affects people's health at the same time. Among which, ammonia (NH_3) is a common gas that widely exists in industrial processes, fertilizer productions, food processing, and explosives (e.g., NH_4NO_3).[1−6] Owing to the strong irritation to the respiratory system, skin, and eyes of a human, NH_3 is quite harmful to human health, not only causing acute poisoning when exposed at around 50 ppm of NH_3 gas in air,[7−10] but also related to a certain disease, which can be detected from human breath.[11] Thus, the sensors for monitoring NH_3 with high sensitivity and good selectivity are highly in demand, and there are already plenty of sensors designed for NH_3 detection.[12−15] Nowadays, the portable, wearable, and implantable integrated systems for reversible gas monitoring have attracted extensive interests, which are widely applied in real-time monitoring of target gas to control industrial processes, reduce environmental pollution, and manage physical health.[16−18] However, from an individual gas sensor to its integrated systems, high-response sensing material remains a great challenge to improve sensing performance.

Two-dimensional (2D) materials as a fast-growing family of recently emerging nanomaterials have attracted immense research interests in many fields, such as catalysis, supercapacitor, photoelectric device, and sensor.[19−21] Although remarkable properties could be observed in 2D nanomaterials due to their unique structure with one dimension restricted to few-atom layers while other dimension could be up to a few micrometers,[19] there are still some existing drawbacks such as a relatively low specific surface area and reduced performance owing to the uncontrollable layer restacking.[22,23] Especially for sensors, a single 2D material is always difficult to satisfy our needs, for example, graphene possesses outstanding electrical conductivity but is insusceptible for sensors, while conducting polymer (CPs) nanosheets are sensitive to target gas but inferior to graphene in terms of electrical conductivity. To overcome this issue, 2D heterostructures assembled with graphene and CPs nanosheets by a sandwich-like structure and

Received: June 14, 2020
Accepted: July 31, 2020
Published: July 31, 2020

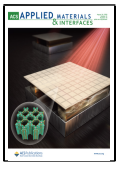

https://dx.doi.org/10.1021/acsami.0c10794
ACS Appl. Mater. Interfaces 2020, 12, 38674−38681

accompanied by the introduction of mesopores at the same time undoubtedly guarantee a preferable sensing behavior, which is attributed to the strong synergistic effect of graphene and CPs to enhance the specific surface area from the mesoporous structure and speed up the carrier transport. As far as we know, the intrinsic structure−property relationship referring to how the size and structure of mesopores in a 2D heterostructure affect the sensing property is still unexplored.

In this work, we have developed a highly sensitive gas sensor for the fast detection of NH_3 at room temperature based on 2D wormlike mesoporous polypyrrole layers stacked on free-standing reduced graphene oxide (rGO) nanosheets (denoted as w-mPPy@rGO). Notably, the resulting w-mPPy@rGO heterostructures displayed greatly improved sensing behavior compared with the other two counterparts (spherical mesoporous PPy@rGO and nonporous PPy@rGO) due to their large specific surface areas (193 m^2/g) and unique mesoporous structures, which offered a pathway for effective gas diffusion and thus helped for fast response and recovery. The w-mPPy@rGO heterostructures delivered higher response (42% to 10 ppm NH_3) with a limit-of-detection (LOD) of 41 ppb based on $3\sigma/k$ (σ represents the standard deviation of the baseline and k corresponds to the slope of the standard curve). Moreover, the chemosensor based on w-mPPy@rGO heterostructures demonstrated superb selectivity toward common volatile organic compounds (VOCs), H_2S, and CO, together with prominent stability for NH_3 detection without the interference of humidity (<65%). Finally, a self-powered sensor system consisting of a layered triboelectric nanogenerator, a lithium-ion battery, and a w-mPPy@rGO-based sensor was constructed as a portable and light-weight sensing device for sensitive, selective, reversible, and steady NH_3 wireless monitoring. More importantly, our self-powered sensor system showed substantially increased resistance ($\Delta R/R_0$ = 17%) toward 5 mg of NH_4NO_3 as we had expected before, signifying its potential use in NH_3-based detection aspect.

EXPERIMENTAL SECTION

Materials. All of the chemicals were purchased from Sinopharm Chemical Reagent Co., Ltd and were of analytical grade. All reagents were of commercial quality and used without further purification.

Characterization. Scanning electron microscopy (SEM) was performed on a JSM-7800F (Japan) instrument. Transmission electron microscopy (TEM) and high-resolution TEM (HRTEM) were conducted on a JEM-2100 instrument. Atomic force microscopy (AFM) was performed on a Cypher ES instrument. Raman spectra were measured on LabRAM HR 800, 532 nm. Fourier-transform infrared spectra (FT-IR) were obtained on Bruker Optics hyperion 3000. N_2 adsorption/desorption isotherms were conducted on TriStar II 3020. The specific surface area and the pore size distribution were evaluated using the Brunauer−Emmett−Teller (BET) and Barrett−Joyner−Halenda (BJH) methods, respectively. The chemical component was characterized by X-ray photoelectron spectroscopy (XPS) with Thermo ESCALAB 250.

Synthesis of Materials. Graphene oxide (GO) was synthesized from graphite flakes using the modified Hummers method.[24,25]

The w-mPPy@GO heterostructures were synthesized using a soft template method.[26] Specifically, the pyrrole was in situ polymerized on a 2D GO surface, and poly(ethylene oxide)-*b*-poly(propylene oxide)-*b*-poly(ethylene oxide) triblock copolymer (P123) micelles were utilized as a mesoporous template. First, 0.5 g of P123 was dissolved in 2 mL of tetrahydrofuran and 16 mL of deionized water to form wormlike aggregation. After stirring for 1 h, 2 mL of GO (1.5 mg/mL) was added into the solution. Next, 60 μL of pyrrole and 180 mg of ammonium persulfate were added to initiate polymerization of pyrrole. After washing and centrifugation, w-mPPy@GO was obtained. Then, w-mPPy@rGO heterostructures were obtained via the reduction of w-mPPy@GO by hydrothermal treatment at 180 °C for 12 h followed by HCl (1 M) doping overnight.

For comparison, the spherical mesoporous polypyrrole/rGO (s-mPPy@rGO) nanosheets were synthesized by employing polystyrene-*b*-poly(ethylene oxide) (PS_{100}-*b*-PEO_{115}) as the mesoporous template instead of P123, and other procedures were kept the same as w-mPPy@rGO.

The nonporous polypyrrole/rGO (n-PPy@rGO) nanosheets were synthesized without using the mesoporous template, and other steps were the same as w-mPPy@rGO.

Fabrication of the Gas Sensor. Typically, 2D w-mPPy@rGO heterostructures were dispersed in ethanol and sonicated for several minutes to obtain the suspension (1 mg/mL). Then, 20 μL of the slurry was drop-coated on a ceramic tube where two Au electrodes were printed on and connected with two wires. Gas sensing measurements were conducted in a 18 L homemade seal chamber, which includes a heating block to evaporate ammonium hydroxide; the schematic diagram of the seal chamber and sensor are shown in Figure S1 (Supporting Information), together with the method for calculation of gas concentration. The gas response is defined as (eq 1)

$$\frac{\Delta R}{R_0} = \frac{R - R_0}{R_0} \times 100\% \quad (1)$$

Or the gas response is defined as (eq 2)

$$\frac{\Delta I}{I_0} = \frac{I_0 - I}{I_0} \times 100\% \quad (2)$$

where R (I) and R_0 (I_0) are the real-time and initial resistances (or currents), respectively. The response and recovery time are defined as the times at which the sensor reaches 90% of the total resistance (or current) change.

Fabrication of the Nanogenerator and the Lithium-Ion Battery. A layered triboelectric nanogenerator was fabricated according to the previous literature with some modifications.[27] Typically, a Kapton film with a thickness of 125 μm was folded into a zigzag with 20 layers and served as the substrate. Then, a Cu film with an area of 5 cm × 5 cm was adhered to both sides of the Kapton film. Then, PTFE tapes were attached on both sides of the Cu layer every other layer in a symmetrical structure. The short-circuit current was recorded by a Source Meter (Model 2450), and the open-circuit voltage was obtained via an oscilloscope (UNI-I UTD2202 CM).

As for the battery, the commercially available $LiFePO_4$ (LFP) and $Li_4Ti_5O_{12}$ (LTO) powders were mixed and grinded with a poly(vinylidene fluoride) (PVDF) binder, conductive carbon black (8:1:1, weight ratio) in *N*-methyl pyrrolidone (NMP) to prepare cathode and anode slurries respectively, which were then blade-coated on carbon-coated Al and Cu foils and dried under vacuum at 100 °C for 12 h. Circular electrodes with a diameter of 12 mm were obtained using a punch machine. The coin cells (CR 2016) were assembled in an Ar-filled glovebox ($c(H_2O)$ < 0.5 ppm, $c(O_2)$ < 0.5 ppm) with an LTO anode, an LFP cathode, a polypropylene separator, and 1 M $LiPF_6$ in ethylene carbonate (EC)/dimethyl carbonate (DMC) electrolyte. The galvanostatic charge/discharge tests with different current densities were conducted within the voltage range of 1−2.4 V using a LAND-CT2001A battery tester at room temperature.

RESULTS AND DISCUSSION

Structural and Morphological Characterization. The schematic fabrication processes of w-mPPy@rGO, s-mPPy@rGO, and n-PPy@rGO nanosheets are shown in Scheme S1 (Supporting Information). Taking w-mPPy@rGO as an example, first, P123 was stirred to generate the wormlike micelle, which was absorbed on GO surface through the hydrogen-bond interaction. Then, w-mPPy@GO heterostructures were prepared by in situ polymerization of pyrrole on the

https://dx.doi.org/10.1021/acsami.0c10794
ACS Appl. Mater. Interfaces 2020, 12, 38674−38681

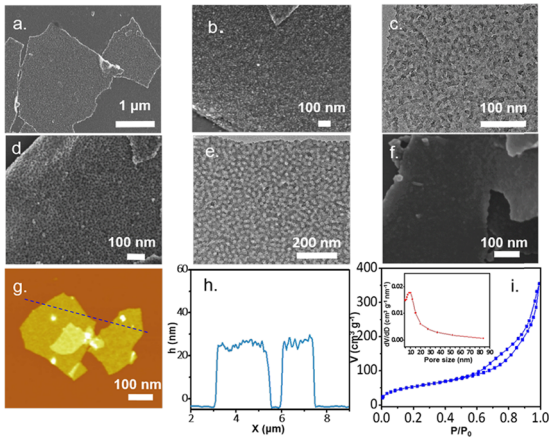

Figure 1. (a, b) SEM and (c) TEM images of 2D w-mPPy@rGO heterostructures. (d) SEM and (e) TEM images of 2D s-mPPy@rGO heterostructures. (f) SEM image of n-PPy@rGO heterostructures. (g, h) AFM topography image and the corresponding thickness information of w-mPPy@rGO heterostructures. (i) N_2 adsorption/desorption isotherm, and the inset showing the pore size distribution of w-mPPy@rGO heterostructures.

surface of P123 micelle−GO nanosheets. Finally, the reduction of mPPy@GO by hydrothermal treatment was performed to yield w-mPPy@rGO heterostructures. When the soft template P123 was replaced by PS-PEO, spherical micelles were readily formed, which at last contributed to s-mPPy@rGO. It is worth noting that if no template was added, n-PPy@rGO hybrids with no pores and stacked structure tended to appear. The usage of different templates yielded different mesoporous structures, highlighting the essential role of templates for the formation of specific mesopores. The structure and morphology of the as-prepared w-mPPy@rGO heterostructures are characterized in detail in Figures 1 and S2. As shown in Figure

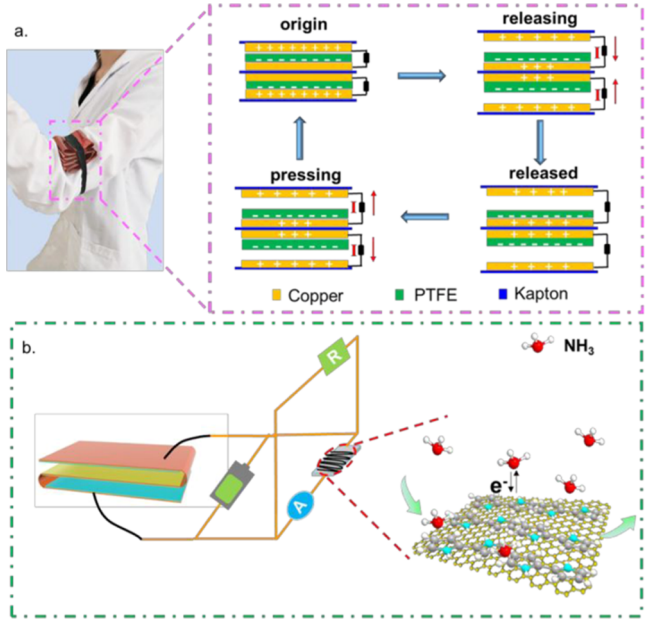

Figure 3. (a) Diagrams of layered TENG. (b) Test circuit and the sensing process toward NH_3 in NH_4NO_3.

1a,b, w-mPPy@rGO heterostructures displayed a flat, uniform 2D morphology with well-ordered, wormlike mesopores on a graphene substrate through the SEM observation. TEM images also revealed the homogeneous mesoporous structures of w-mPPy@rGO, which were in accord with the SEM results (Figure 1c). In contrast, s-mPPy@rGO displayed spherical mesoporous structures through SEM and TEM (Figure 1d,e), while n-PPy@rGO exhibited nonporous structures (Figure 1f), unveiling the successful synthesis of different polypyrrole/graphene heterostructures. Besides, the AFM image and height

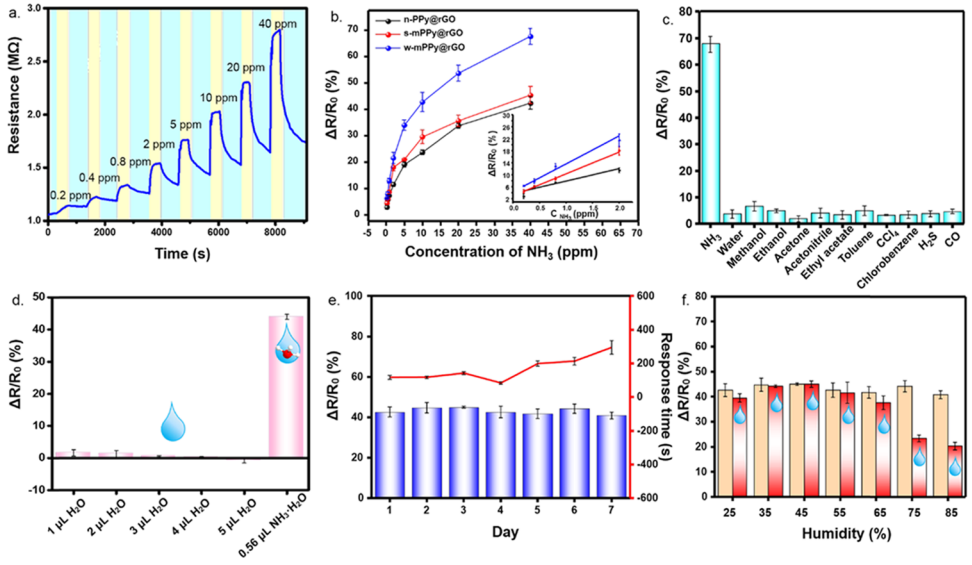

Figure 2. (a) Real-time dynamic resistance responses of 2D w-mPPy@rGO heterostructures toward NH_3 in varying concentrations of 0.2−40 ppm at room temperature. (b) Response comparison of w-mPPy@rGO heterostructures, s-mPPy@rGO and n-PPy@rGO toward 0.2−40 ppm NH_3, and the inset showing a linear relationship between the response and concentration of NH_3 in the range of 0.2−2 ppm NH_3. (c) Selectivity of w-mPPy@rGO heterostructures toward NH_3 with 40 ppm, other common VOCs with 500 ppm, and H_2S and CO with 100 ppm, respectively. (d) Effect of water in aqua ammonia for the sensor. (e) Stability of the sensor toward 10 ppm NH_3 in 7 days (left coordinate) and the corresponding response time (right coordinate). (f) Response comparison of w-mPPy@rGO heterostructures to 10 ppm NH_3 between 20% humidity (left bar) and humidity from 25 to 85% (right bar).

https://dx.doi.org/10.1021/acsami.0c10794
ACS Appl. Mater. Interfaces 2020, 12, 38674−38681

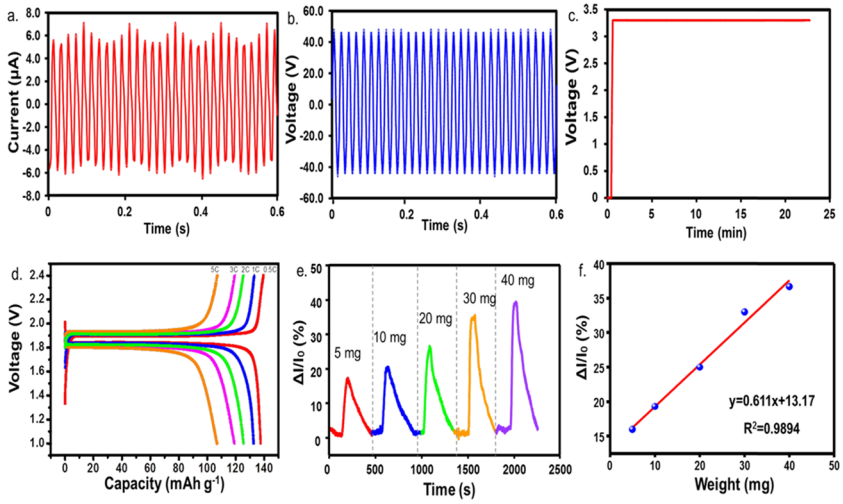

Figure 4. Curves of the short-circuit current (a) and open-circuit voltage (b) of the as-prepared TENG changing with time. (c) Voltage integrated by the energy conversion module increasing to 3.3 V with a long time. (d) Charge−discharge profiles at 0.5C, 1C, 2C, 3C, and 5C for the LTO/LFP full cell. (e) Current response of the sensor toward different amounts of NH_4NO_3 from 5 to 40 mg. (f) Linear relationship between the current response ($\Delta I/I_0$) and different weights of NH_4NO_3 from 5 to 40 mg.

analysis exhibited that w-mPPy@rGO heterostructures possessed an ultrathin 2D structure with an uniform thickness of ∼30 nm, as seen in Figure 1g,h. N_2 adsorption/desorption isotherm was conducted to investigate the mesoporous feature and the specific surface area of w-mPPy@rGO, and the narrow pore size distribution calculated by the BJH method presented an average pore size of ∼10 nm, consistent with SEM and TEM observations (Figure 1i). The specific surface area and pore volume were calculated to be 193 m^2/g and 0.516 cm^3/g, respectively. The relatively large surface area amplified the target−receptor interface, which is beneficial to gas diffusion, accelerating the response and recovery speed of the sensor consequently. Moreover, the FT-IR spectrum of w-mPPy@rGO heterostructures showed typical vibration peaks of polypyrrole and rGO, including the characteristic peaks of C═C bond at 1550 and 1470 cm^{-1}, N−H group at 1645 and 1375 cm^{-1}, C−N bond at 1279 cm^{-1}, and C−H group at 1035 cm^{-1},[28,29] as shown in Figure S2a, demonstrating the successful hybridization of rGO and PPy in w-mPPy@rGO heterostructures. It is found that from the Raman spectrum, the D and G peaks of graphene centered at 1350 and 1590 cm^{-1} were overlapped with the peaks of polypyrrole at 1340 and 1570 cm^{-1} corresponding to C═C stretching modes (Figure S2b).[16,26,28,30] In addition, the higher intensity ratio (I_D/I_G) of 1.03 for w-mPPy@rGO nanosheets than that (I_D/I_G = 0.99) before reduction, is indicative of the effective reduction of the GO interlayer.[26,31−36]To better understand the chemical composition of w-mPPy@rGO heterostructures, XPS spectra were also collected (Figure S2c,d). The C1s main peak was decomposed into five individual peaks at 284.1, 285.1, 286.2, 287.8, and 290.4 eV, corresponding to β-carbons and α-carbons in pyrrole rings, polarons, bipolarons, and the $\pi-\pi^*$ satellite of aromatic PPy, respectively. The deconvolution of N1s signals in the XPS spectrum gave three peaks, in which the main N peak at 399.6 eV was attributed to the neutral N in the Py ring (−NH−), the peak at 400.5 eV was indicative of $-NH^{\bullet+}-$ in the polaron charge carrier species, and the peak at 402.5 eV could be assigned to $=NH^{+}-$, a bipolaron charge carrier species.[37,38] In addition, other relevant characterizations of s-mPPy@rGO and n-PPy@rGO are given in Figures S3 and S4.

Gas Sensing Properties. To verify the influence of pore structures and morphologies on sensing performance, w-mPPy@rGO, s-mPPy@rGO, and n-PPy@rGO were tested under the same conditions. In Figure 2a, the real-time dynamic resistance responses of w-mPPy@rGO heterostructures toward ammonia in varying concentrations of 0.2−40 ppm at room temperature were measured. Evidently, the resistance of w-mPPy@rGO heterostructures was substantially increasing upon exposure to NH_3, elucidating the typical p-type semiconductor behavior for reducing gas.[18,39] The whole sensing process was less than 200 s followed by exchanging of fresh air, and the resistance approximately recovered within 10 min. The short response and recovery time were attributed to the large specific surface areas of w-mPPy@rGO heterostructures, which could accelerate gas diffusion and carrier transport. Moreover, w-mPPy@rGO heterostructures exhibited a remarkably enhanced response ($\Delta R/R_0$ = 45% for 10 ppm NH_3) than the other two counterparts (s-mPPy@rGO and n-PPy@rGO) from 0.2 to 40 ppm NH_3 (Figures 2b, S5, and S6). Together with good linear regression between the response of a sensor and concentration of NH_3 from 0.2 to 2 ppm, the LOD of w-mPPy@rGO heterostructures was calculated to be 41 ppb based on $3\sigma/k$, where σ represents the standard deviation of the baseline and k corresponds to the slope of the standard curve (Figure 2b). Meanwhile, the sensing performance of our w-mPPy@rGO-based sensor is in excess of most reported sensors based on polymer or polymer/graphene composites in terms of response value, response/recovery times, and limit-of-detection (LOD) (Table S1, Supporting Information). To gain a deep insight into the prominent sensing performance of 2D w-mPPy@rGO heterostructures, specific surface areas of these three materials are compared, showing a higher specific surface area of 193 m^2/g for w-mPPy@rGO in comparsion with s-mPPy@rGO (138 m^2/g) and n-PPy@rGO (125 m^2/g). Taking all of the above mentioned points into consideration, it is speculated that the synergistic effect of the large specific surface area and typical wormlike mesopores in a w-mPPy@rGO hetero-

https://dx.doi.org/10.1021/acsami.0c10794
ACS Appl. Mater. Interfaces 2020, 12, 38674−38681

structure plays a key role in inducing an outstanding response, which promotes the gas diffusion and carrier transport, and thus realizes high response signals.

To evaluate the anti-interference property of a sensor, the cross response of w-mPPy@rGO heterostructures to some other interfering gases including common volatile organic compounds (VOCs) such as methanol, ethanol, acetone, acetonitrile, ethylacetate, toluene, carbon tetrachloride, chlorobenzene, and inorganic gases such as water, H_2S, and CO were tested to explore its selectivity. In contrast tests, the concentration of VOCs was 500 and 100 ppm for H_2S and CO, while the concentration of NH_3 was just 40 ppm. As shown in Figure 2c, w-mPPy@rGO heterostructures exhibit much higher response toward NH_3 than other mentioned gases, reflecting the desirable anti-interference performance. In addition, because the sensing experiments were conducted by evaporating aqua ammonia to release gaseous NH_3, the effect of water should not be ignored. Different amounts of water (1−5 μL) were added to the homemade seal chamber, and then heated to evaporate; negligible variation of resistance was observed compared with the addition of 0.56 μL of 25% ammonium hydroxide (corresponding to 10 ppm NH_3) (Figure 2d), demonstrating that water in aqua ammonia has little effect on the whole sensing process. To illustrate the reproducibility of the sensor, a w-mPPy@rGO heterostructure-based sensor was evaluated during periodic exposures to 10 ppm NH_3 every 24 h for 7 days. It is indicated that the response values almost remain at 40% in seven cycles along with a short response time less than 400 s, revealing superior reversibility and favorable repeatability of the w-mPPy@rGO-based sensor, as seen in Figure 2e. As far as we know, it remains a great challenge for a polymer-based sensor working in a high humidity atmosphere,[40] and the antihumidity property of the sensor is a vital parameter for the real application, thus antihumidity interference tests of a w-mPPy@rGO-based sensor were also carried out. Different humidity atmospheres were generated by injecting various amounts of water into the chamber monitored by a hygrometer. It is clearly seen that under relative humidity from 25 to 65%, there was almost no influence on the response of the w-mPPy@rGO-based sensor. When the humidity was higher than 65%, an obvious response reduction came out, which could be ascribed to gaseous NH_3 redissolved in water in high humidity, leading to a lower concentration of gaseous NH_3 than the theoretical value (Figure 2f).

Sensing Mechanism of the w-mPPy@rGO-Based Sensor. The sensing mechanism of 2D w-mPPy@rGO is ascribed to the following factors: first, PPy as a typical p-type semiconductor owns the hole conduction property.[41,42] When the electron-donating NH_3 molecules adsorb onto the PPy surface, the electrons transfer from NH_3 to the π backbone of PPy, which undoubtedly reduces the hole in PPy, and thus increases the resistance of PPy. As for the desorption process, the electrons return from PPy to NH_3, leading to the recovery of PPy resistance.[37,43,44] Further, with respect to the whole sensing process, the outstanding electrical conductivity of rGO as well as the affinity of PPy and rGO is favorable for effective electron conduction during the sensing process. Besides, rGO consists of a large amount of sp^2-bonded carbons, vacancies, structural defects, and residual oxygen groups. They create a hole-transporting matrix, acting as a p-type semiconductor as well.[45] The absorbed NH_3 molecules in the sensing process are able to transfer electrons onto the surface of rGO too, resulting in the increment of resistance. Overall, the synergistic effect of p-type PPy and rGO plays a key role in NH_3 sensing. In addition, the prominent conductivity of rGO behaving as a bridge for electronic transmission and the large specific surface area of w-mPPy@rGO beneficial to fast adsorption/desorption further improve sensing performance consequently.

Self-Powered Sensor System for the Detection of NH_4NO_3. To realize wireless, portable, sustainable, and self-powered NH_3 detection for practical application, the integration of an energy harvesting device, an energy storing device, and a NH_3 sensor is highly required to achieve this goal. As is known to all, the triboelectric nanogenerators (TENG) as a kind of energy harvest device could harvest electrical energy from the environmental mechanical energy or human mechanical energy, and it can provide a safe, effective, and eco-friendly way to drive portable electronics.[46−48] Till now, TENG has been widely investigated in many fields, such as motion detection, pressure measurement, and chemical sensing area.[49−52] As for the energy storing device, we choose a lithium-ion battery owing to its advantages of high voltage, high energy density, long cycling life, and good environmental compatibility, which is usually used as a convenient power source for portable electronics.[53] Consequently, a self-powered sensor system assembled with TENG, a lithium-ion battery (LTO/LFP), and a w-mPPy@rGO heterostructure-based sensor was successfully applied to explosive detection, in which NH_4NO_3 was selected as the target readily releasing NH_3 via alkaline decomposition. The schematic diagrams of TENG and the sensing process of NH_3 in NH_4NO_3 are clearly shown in Figure 3a,b. Typically, as for the layered TENG in the initial state, with an external force, the TENG is compressed till the PTFE film and the metal electrode contact each other tightly. Due to different electron-withdrawing abilities, the PTFE surface is negatively charged resultantly. Then, after releasing the force, the electrons on the back electrode transfer to the metal electrode through an external load driven by the electrostatic induction. Next, in the released state, electrons stop flowing when the electrostatic equilibrium is formed. Finally, when the TENG is compressed again, electrons transfer from the metal electrode to the back electrode until film surfaces touch closely again in line with the initial state.[27] The curves of the short-circuit current and open-circuit voltage of the as-prepared TENG changing with time are shown in Figure 4a,b, the values of which are both high, so the obtained power value is sufficient enough to drive the energy conversion module. The voltage integrated by the energy conversion module increased to 3.3 V immediately, which could steadily charge the battery used in this experiment for a long time (Figure 4c). Once charged by layered triboelectric nanogenerators, the LTO/LFP full battery exhibited a specific capacity of 135 mAh/g (Figures 4d and S7, based on the mass of LFP) and stable cycle performance at 1 C (Figure S8), demonstrating satisfying rate capability and cycling performance of this energy storage device. Then, the battery was employed to drive a w-mPPy@rGO-based sensor and connected to a multiple circuit with an amperemeter and external load resistance (Figure 3b). Afterward, different amounts of NH_4NO_3 were added to the seal chamber followed by alkaline hydrolysis via 1 mol/L NaOH, and the current signal was recorded. It could be clearly seen that dynamic current changed with the weight of NH_4NO_3 with good linear regression between the current response and weight of NH_4NO_3, and the response toward 5 mg of NH_4NO_3 could

https://dx.doi.org/10.1021/acsami.0c10794
ACS Appl. Mater. Interfaces 2020, 12, 38674−38681

reach 17%, indicating high sensitivity and superiority of the as-fabricated integrated system, as seen in Figure 4e,f. Therefore, the self-powered sensor system composed of TENG, a lithium-ion battery, and a w-mPPy@rGO-based sensor holds great promise to realize in situ determination of NH_3-based analytes with fast response, convenient operation, and cost-efficiency.

CONCLUSIONS

In summary, 2D wormlike mesoporous polypyrrole/graphene heterostructures were demonstrated for an ultrasensitive NH_3 sensor and its self-powered integrated system. The resulting 2D w-mPPy@rGO-based sensor displayed remarkable response ($\Delta R/R_0$ = 45% for 10 ppm NH_3 with LOD of 41 ppb) toward 0.2−40 ppm gaseous NH_3, demonstrating its fast gas diffusion and transport of carriers owing to a large specific surface area (193 m^2/g) and an unique mesoporous structure. Moreover, a 2D w-mPPy@rGO-based sensor disclosed prominent selectivity toward VOCs, H_2S, and CO, favorable antihumidity performance, and easy operation at room temperature. Remarkably, an independent, miniaturized, sustainable integrated system assembled with layered TENG, a lithium-ion battery, and a w-mPPy@rGO-based sensor was constructed to sensitively monitor NH_4NO_3 as an example. High response and favorable linear regression between the current response and weight of NH_4NO_3 make our self-powered sensor system a prospective tool in the NH_3-related sensing field. Our research not only paves a new way in 2D mesoporous heterostructures employed in sensing materials, but also gives a guide to creating the miniaturized, flexible, self-powered electronics for toxic gas monitoring, environmental protection, and personalized healthcare.

ASSOCIATED CONTENT

Supporting Information

The Supporting Information is available free of charge at https://pubs.acs.org/doi/10.1021/acsami.0c10794.

Synthesis process of PPy@rGO with different porous structures and morphologies; the sensing performance comparison of w-mPPy/rGO heterostructures with the previously reported conducting polymers; the schematic diagram of the seal chamber and sensor; the FT-IR spectrum, the Raman spectrum, and XPS spectra of w-mPPy@rGO heterostructures; relevant characterizations of s-mPPy@rGO nanosheets and n-PPy@rGO; the real-time dynamic resistance responses toward NH_3 of s-mPPy@rGO and n-PPy@rGO; and the rate performance of the LFP/LTO lithium-ion battery and the cycling stability of LFP/LTO full cell measured at 1C (PDF)

AUTHOR INFORMATION

Corresponding Authors

Zhong-Shuai Wu − *State Key Laboratory of Catalysis, Chinese Academy of Sciences, Dalian 116023, China; Dalian National Laboratory for Clean Energy, Dalian Institute of Chemical Physics, Chinese Academy of Sciences, Dalian 116023, China;* orcid.org/0000-0003-1851-4803; Email: wuzs@dicp.ac.cn

Liang Feng − *Department of Instrumentation and Analytical Chemistry, CAS Key Laboratory of Separation Science for Analytical Chemistry, Dalian Institute of Chemical Physics, Chinese Academy of Sciences, Dalian 116023, China;* orcid.org/0000-0002-7586-8424; Email: fengl@dicp.ac.cn

Authors

Jianmei Gao − *Department of Instrumentation and Analytical Chemistry, CAS Key Laboratory of Separation Science for Analytical Chemistry, Dalian Institute of Chemical Physics, Chinese Academy of Sciences, Dalian 116023, China; University of Chinese Academy of Sciences, Beijing 100049, China*

Jieqiong Qin − *State Key Laboratory of Catalysis, Chinese Academy of Sciences, Dalian 116023, China; Dalian National Laboratory for Clean Energy, Dalian Institute of Chemical Physics, Chinese Academy of Sciences, Dalian 116023, China; University of Chinese Academy of Sciences, Beijing 100049, China*

Junyu Chang − *Department of Instrumentation and Analytical Chemistry, CAS Key Laboratory of Separation Science for Analytical Chemistry, Dalian Institute of Chemical Physics, Chinese Academy of Sciences, Dalian 116023, China; University of Chinese Academy of Sciences, Beijing 100049, China*

Hanqing Liu − *State Key Laboratory of Catalysis, Chinese Academy of Sciences, Dalian 116023, China; Dalian National Laboratory for Clean Energy, Dalian Institute of Chemical Physics, Chinese Academy of Sciences, Dalian 116023, China; University of Chinese Academy of Sciences, Beijing 100049, China*

Complete contact information is available at: https://pubs.acs.org/10.1021/acsami.0c10794

Author Contributions

⊥J.G. and J.Q. contributed equally to this work.

Notes

The authors declare no competing financial interest.

ACKNOWLEDGMENTS

The authors acknowledge the financial support from the Key Project of CAS (KFJ-STS-ZDTP-083), Dalian Distinguished Young Scholars (2018RJ02), the National Key R&D Program of China (2016YFA0200200), the National Natural Science Foundation of China (51702078, 51572259, and 51872283), the Natural Science Foundation of Liaoning Province, Joint Research Fund Liaoning-Shenyang National Laboratory for Materials Science (20180510038), the Liaoning Revitalization Talents Program (XLYC1807153), DICP (ZZBS201708, ZZBS201802, and DICP I202032), DICP&QIBEBT (UN201702), and the Dalian National Laboratory For Clean Energy (DNL), CAS, DNL Cooperation Fund, CAS (DNL180310, DNL180308, DNL201912, and DNL201915).

ABBREVIATIONS

w-mPPy@rGO, wormlike mesoporous polypyrrole/reduced graphene oxide
s-mPPy@rGO, spherical mesoporous polypyrrole/reduced graphene oxide
n-PPy@rGO, nonporous polypyrrole/reduced graphene oxide
LOD, limit-of-detection
VOCs, volatile organic compounds
TENG, triboelectric nanogenerator

REFERENCES

(1) Zhang, D. Z.; Wu, Z. L.; Zong, X. Q.; Zhang, Y. Fabrication of Polypyrrole/Zn2SnO4 Nanofilm for Ultra-highly Sensitive Ammonia Sensing Application. *Sens. Actuators, B* **2018**, *274*, 575−586.

(2) Zhang, D. Z.; Jiang, C. X.; Li, P.; Sun, Y. E. Layer-by-Layer Self-Assembly of Co3O4 Nanorod-Decorated MoS2 Nanosheet-Based Nanocomposite toward High-Performance Ammonia Detection. *ACS Appl. Mater. Interfaces.* **2017**, *9*, 6462−6471.

(3) Kumar, L.; Rawal, I.; Kaur, A.; Annapoorni, S. Flexible Room Temperature Ammonia Sensor Based on Polyaniline. *Sens. Actuators, B* **2017**, *240*, 408−416.

(4) Li, Y.-P.; Li, S.-N.; Jiang, Y.-C.; Hu, M.-C.; Zhai, Q.-G. A Semiconductor and Fluorescence Dual-Mode Room-Temperature Ammonia Sensor Achieved by Decorating Hydroquinone into a Metal-Organic Framework. *Chem. Commun.* **2018**, *54*, 9789−9792.

(5) Assen, A. H.; Yassine, O.; Shekhah, O.; Eddaoudi, M.; Salama, K. N. MOFs for the Sensitive Detection of Ammonia: Deployment of fcu-MOF Thin Films as Effective Chemical Capacitive Sensors. *ACS Sens.* **2017**, *2*, 1294−1301.

(6) Travlou, N. A.; Singh, K.; Rodriguez-Castellon, E.; Bandosz, T. J. Cu−BTC MOF−Graphene-Based Hybrid Materials as Low Concentration Ammonia Sensors. *J. Mater. Chem. A* **2015**, *3*, 11417−11429.

(7) Joshi, A.; Gangal, S. A.; Gupta, S. K. Ammonia Sensing Properties of Polypyrrole Thin Films at Room Temperature. *Sens. Actuators, B* **2011**, *156*, 938−942.

(8) Liu, X.; Chen, N.; Han, B. Q.; Xiao, X. C.; Chen, G.; Djerdj, I.; Wang, Y. D. Nanoparticle Cluster Gas Sensor: Pt Activated SnO2 Nanoparticles for NH3 Detection with Ultrahigh Sensitivity. *Nanoscale* **2015**, *7*, 14872−14880.

(9) Yin, Y.; Zhang, H. T.; Huang, P. R.; Xiang, C. L.; Zou, Y. J.; Xu, F.; Sun, L. X. Inducement of Nanoscale Cu-BTC on Nanocomposite of PPy−rGO and its Performance in Ammonia Sensing. *Mater. Res. Bull.* **2018**, *99*, 152−160.

(10) Wang, J.; Yang, P.; Wei, X. W. High-Performance, Room-Temperature, and No-Humidity-Impact Ammonia Sensor Based on Heterogeneous Nickel Oxide and Zinc Oxide Nanocrystals. *ACS Appl. Mater. Interfaces* **2015**, *7*, 3816−3824.

(11) Tang, X. H.; Lahem, D.; Raskin, J.-P.; Gerard, P.; Geng, X.; Andre, N.; Debliquy, M. A Fast and Room-Temperature Operation Ammonia Sensor Based on Compound of Graphene with Polypyrrole. *IEEE Sens. J.* **2018**, *18*, 9088−9096.

(12) Zhang, D. Z.; Yang, Z. M.; Li, P.; Pang, M. S.; Xue, Q. Z. Flexible Self-Powered High-Performance Ammonia Sensor Based on Au Decorated MoSe2 Nanoflowers Driven by Single Layer MoS2-Flake Piezoelectric Nanogenerator. *Nano Energy* **2019**, *65*, No. 103974.

(13) Zhang, D. Z.; Li, Q.; Li, P.; Pang, M. S.; Luo, Y. W. Fabrication of Pd-Decorated MoSe2 Nanoflowers and Density Functional Theory Simulation Toward Ammonia Sensing. *IEEE Electron Device Lett.* **2019**, *40*, 616−619.

(14) Zhang, D. Z.; Wu, Z. L.; Li, P.; Zong, X. Q.; Dong, G. K.; Zhang, Y. Facile Fabrication of Polyaniline/Multi-Walled Carbon Nanotubes/Molybdenum Disulfide Ternary Nanocomposite and its High-Performance Ammonia-Sensing at Room Temperature. *Sens. Actuators, B* **2018**, *258*, 895−905.

(15) Zhang, D. Z.; Liu, J. J.; Jiang, C. X.; Liu, A. M.; Xia, B. K. Quantitative Detection of Formaldehyde and Ammonia Gas via Metal Oxide-Modified Graphene-Based Sensor Array Combining with Neural Network Model. *Sens. Actuators, B* **2017**, *240*, 55−65.

(16) Qin, J. Q.; Gao, J. M.; Shi, X. Y.; Chang, J. Y.; Dong, Y. F.; Zheng, S. H.; Wang, X.; Feng, L.; Wu, Z.-S. Hierarchical Ordered Dual-Mesoporous Polypyrrole/Graphene Nanosheets as Bi-Functional Active Materials for High-Performance Planar Integrated System of Micro-Supercapacitor and Gas Sensor. *Adv. Funct. Mater.* **2020**, *30*, No. 1909756.

(17) Nazemi, H.; Joseph, A.; Park, J.; Emadi, A. Advanced Micro- and Nano-Gas Sensor Technology: A Review. *Sensors* **2019**, *19*, 1285.

(18) Wagner, T.; Haffer, S.; Weinberger, C.; Klaus, D.; Tiemann, M. Mesoporous Materials as Gas Sensors. *Chem. Soc. Rev.* **2013**, *42*, 4036−4053.

(19) Zhu, J.; Ha, E. N.; Zhao, G. L.; Zhou, Y.; Huang, D. H.; Yue, G. Z.; Hu, L. S.; Sun, N.; Wang, Y.; Lee, L. Y. S.; Xu, C.; Wong, K.-Y.; Astruc, D.; Zhao, P. X. Recent Advance in MXenes: A Promising 2D Material for Catalysis, Sensor and Chemical Adsorption. *Coord. Chem. Rev.* **2017**, *352*, 306−327.

(20) Mas-Balleste, R.; Gomez-Navarro, C.; Gomez-Herrero, J.; Zamora, F. 2D Materials: To Graphene and Beyond. *Nanoscale* **2011**, *3*, 20−30.

(21) Tan, C. L.; Cao, X. H.; Wu, X.-J.; He, Q. Y.; Yang, J.; Zhang, X.; Chen, J. Z.; Zhao, W.; Han, S. K.; Nam, G.-H.; Sindoro, M.; Zhang, H. Recent Advances in Ultrathin Two-Dimensional Nanomaterials. *Chem. Rev.* **2017**, *117*, 6225−6331.

(22) Li, Y. P.; Zhao, R.; Shi, L. Y.; Han, G. Y.; Xiao, Y. M. Acetylcholinesterase Biosensor Based on Electrochemically Inducing 3D Graphene Oxide Network/Multi-Walled Carbon Nanotube Composites for Detection of Pesticides. *RSC Adv.* **2017**, *7*, 53570−53577.

(23) Zhang, Q.; Huang, J.-Q.; Qian, W.-Z.; Zhang, Y.-Y.; Wei, F. The Road for Nanomaterials Industry: A Review of Carbon Nanotube Production, Post-Treatment, and Bulk Applications for Composites and Energy Storage. *Small* **2013**, *9*, 1237−1265.

(24) Zhu, Y. W.; Murali, S.; Cai, W. W.; Li, X. S.; Suk, J. W.; Potts, J. R.; Ruoff, R. S. Graphene and Graphene Oxide: Synthesis, Properties, and Applications. *Adv. Mater.* **2010**, *22*, 3906−3924.

(25) Wu, Z.-S.; Zhou, G. M.; Yin, L.-C.; Ren, W. C.; Li, F.; Cheng, H.-M. Graphene/Metal Oxide Composite Electrode Materials for Energy Storage. *Nano Energy* **2012**, *1*, 107−131.

(26) Qin, J. Q.; Zhou, F.; Xiao, H.; Ren, R. Y.; Wu, Z.-S. Mesoporous Polypyrrole-Based Graphene Nanosheets Anchoring Redox Polyoxometalate for All-Solid-State Micro-Supercapacitors with Enhanced Volumetric Capacitance. *Sci. China Mater.* **2017**, *61*, 233−242.

(27) Yin, X.; Liu, D.; Zhou, L. L.; Li, X. Y.; Zhang, C. L.; Cheng, P.; Guo, H. Y.; Song, W. X.; Wang, J.; Wang, Z. L. Structure and Dimension Effects on the Performance of Layered Triboelectric Nanogenerators in Contact-Separation Mode. *ACS Nano* **2019**, *13*, 698−705.

(28) Liu, S. H.; Gordiichuk, P.; Wu, Z.-S.; Liu, Z. Y.; Wei, W.; Wagner, M.; Mohamed-Noriega, N.; Wu, D. Q.; Mai, Y. Y.; Herrmann, A.; Mullen, K.; Feng, X. L. Patterning Two-Dimensional Free-Standing Surfaces with Mesoporous Conducting Polymers. *Nat. Commun.* **2015**, *6*, No. 8817.

(29) Tian, H.; Qin, J. Q.; Hou, D.; Li, Q.; Li, C.; Wu, Z.-S.; Mai, Y. Y. General Interfacial Self-Assembly Engineering for Patterning Two-Dimensional Polymers with Cylindrical Mesopores on Graphene. *Angew. Chem., Int. Ed.* **2019**, *58*, 10173−10178.

(30) Liu, S. H.; Wang, F. X.; Dong, R. H.; Zhang, T.; Zhang, J.; Zhuang, X. D.; Mai, Y. Y.; Feng, X. L. Dual-Template Synthesis of 2D Mesoporous Polypyrrole Nanosheets with Controlled Pore Size. *Adv. Mater.* **2016**, *28*, 8365−8370.

(31) Pei, S. F.; Cheng, H. M. The Reduction of Graphene Oxide. *Carbon* **2012**, *50*, 3210−3228.

(32) Stankovich, S.; Dikin, D. A.; Piner, R. D.; Kohlhaas, K. A.; Kleinhammes, A.; Jia, Y.; Wu, Y.; Nguyen, S. T.; Ruoff, R. S. Synthesis of Graphene-Based Nanosheets via Chemical Reduction of Exfoliated Graphite Oxide. *Carbon* **2007**, *45*, 1558−1565.

(33) Zhou, Y.; Bao, Q. L.; Tang, L. A. L.; Zhong, Y. L.; Loh, K. P. Hydrothermal Dehydration for the "Green" Reduction of Exfoliated Graphene Oxide to Graphene and Demonstration of Tunable Optical Limiting Properties. *Chem. Mater.* **2009**, *21*, 2950−2956.

(34) Shen, J. F.; Yan, B.; Shi, M.; Ma, H. W.; Li, N.; Ye, M. X. One Step Hydrothermal Synthesis of TiO2-Reduced Graphene Oxide Sheets. *J. Mater. Chem.* **2011**, *21*, 3415−3421.

(35) Shen, J. F.; Shi, M.; Yan, B.; Ma, H. W.; Li, N.; Ye, M. X. One-Pot Hydrothermal Synthesis of Ag-Reduced Graphene Oxide Composite with Ionic Liquid. *J. Mater. Chem.* **2011**, *21*, 7795−7801.

https://dx.doi.org/10.1021/acsami.0c10794
ACS Appl. Mater. Interfaces 2020, 12, 38674−38681

(36) Hayes, W. I.; Joseph, P.; Mughal, M. Z.; Papakonstantinou, P. Production of Reduced Graphene Oxide via Hydrothermal Reduction in an Aqueous Sulphuric Acid Suspension and its Electrochemical Behaviour. *J. Solid State Electrochem.* **2014**, *19*, 361−380.
(37) Yoon, T.; Jun, J.; Kim, D. Y.; Pourasad, S.; Shin, T. J.; Yu, S. U.; Na, W.; Jang, J.; Kim, K. S. An Ultra-Sensitive, Flexible and Transparent Gas Detection Film Based on Well-Ordered Flat Polypyrrole on Single-Layered Graphene. *J. Mater. Chem. A* **2018**, *6*, 2257−2263.
(38) Su, N.; Li, H. B.; Yuan, S. J.; Yi, S. P.; Yin, E. Q. Synthesis and Characterization of Polypyrrole Doped with Anionic Spherical Polyelectrolyte Brushes. *Express Polym. Lett.* **2012**, *6*, 697−705.
(39) Bai, H.; Shi, G. Q. Gas Sensors Based on Conducting Polymers. *Sensors* **2007**, *7*, 267−307.
(40) Poghossian, A.; Geissler, H.; Schoning, M. J. Rapid Methods and Sensors for Milk Quality Monitoring and Spoilage Detection. *Biosens. Bioelectron.* **2019**, *140*, No. 111272.
(41) Bazzaoui, M.; Martins, J. I.; Machnikova, E.; Bazzaoui, E. A.; Martins, L. Polypyrrole Films Electrosynthesized on Stainless Steel Grid from Saccharinate Aqueous Solution and its Behaviour toward Acetone Vapor. *Eur. Polym. J.* **2007**, *43*, 1347−1358.
(42) Xue, M. Q.; Li, F. W.; Chen, D.; Yang, Z. H.; Wang, X. W.; Ji, J. H. High-Oriented Polypyrrole Nanotubes for Next-Generation Gas Sensor. *Adv. Mater.* **2016**, *28*, 8265−8270.
(43) Lee, J. S.; Jun, J.; Shin, D. H.; Jang, J. Urchin-Like Polypyrrole Nanoparticles for Highly Sensitive and Selective Chemiresistive Sensor Application. *Nanoscale* **2014**, *6*, 4188−4194.
(44) Kwon, O. S.; Park, S. J.; Yoon, H.; Jang, J. Highly Sensitive and Selective Chemiresistive Sensors Based on Multidimensional Polypyrrole Nanotubes. *Chem. Commun.* **2012**, *48*, 10526−10528.
(45) Tang, X. H.; Raskin, J.-P.; Kryvutsa, N.; Hermans, S.; Slobodian, O.; Nazarov, A. N.; Debliquy, M. An Ammonia Sensor Composed of Polypyrrole Synthesized on Reduced Graphene Oxide by Electropolymerization. *Sens. Actuators, B* **2020**, *305*, No. 127423.
(46) Fan, F.-R.; Tian, Z.-Q.; Wang, Z. L. Flexible Triboelectric Generator! *Nano Energy* **2012**, *1*, 328−334.
(47) Xu, L.; Jiang, T.; Lin, P.; Shao, J. J.; He, C.; Zhong, W.; Chen, X. Y.; Wang, Z. L. Coupled Triboelectric Nanogenerator Networks for Efficient Water Wave Energy Harvesting. *ACS Nano* **2018**, *12*, 1849−1858.
(48) Xu, M. Y.; Zhao, T. C.; Wang, C.; Zhang, S. L.; Li, Z.; Pan, X. X.; Wang, Z. L. High Power Density Tower-like Triboelectric Nanogenerator for Harvesting Arbitrary Directional Water Wave Energy. *ACS Nano* **2019**, *13*, 1932−1939.
(49) Zhao, X.; Kang, Z.; Liao, Q. L.; Zhang, Z.; Ma, M. Y.; Zhang, Q.; Zhang, Y. Ultralight, Self-Powered and Self-Adaptive Motion Sensor Based on Triboelectric Nanogenerator for Perceptual Layer Application in Internet of Things. *Nano Energy* **2018**, *48*, 312−319.
(50) He, C.; Zhu, W. J.; Gu, G. Q.; Jiang, T.; Xu, L.; Chen, B. D.; Han, C. B.; Li, D. C.; Wang, Z. L. Integrative Square-Grid Triboelectric Nanogenerator as a Vibrational Energy Harvester and Impulsive Force Sensor. *Nano Res.* **2017**, *11*, 1157−1164.
(51) Zhao, K.; Gu, G. Q.; Zhang, Y. N.; Zhang, B.; Yang, F.; Zhao, L.; Zheng, M. L.; Cheng, G.; Du, Z. L. The Self-Powered CO2 Gas Sensor Based on Gas Discharge Induced by Triboelectric Nanogenerator. *Nano Energy* **2018**, *53*, 898−905.
(52) Wen, Z.; Chen, J.; Yeh, M.-H.; Guo, H. Y.; Li, Z. L.; Fan, X.; Zhang, T. J.; Zhu, L. P.; Wang, Z. L. Blow-Driven Triboelectric Nanogenerator as an Active Alcohol Breath Analyzer. *Nano Energy* **2015**, *16*, 38−46.
(53) Liu, C.; Li, F.; Ma, L.-P.; Cheng, H.-M. Advanced Materials for Energy Storage. *Adv. Mater.* **2010**, *22*, E28−E62.

https://dx.doi.org/10.1021/acsami.0c10794
ACS Appl. Mater. Interfaces 2020, 12, 38674−38681